Design and Control of a Ball on Ball System With a Programmable Logic Controller and Vision Feedback

Matthias Bibl[*a)] Non-member, Christoph Zech[**] Non-member
Georg Schitter[*] Non-member

In this publication a Ball on Ball setup is modeled, implemented and analyzed. The goal of this setup is to stabilize a ball on top of a second ball in the unstable upper rest position. The position measurement of the upper ball is done optionally by two triangulation sensors or an industrial camera. With the designed control and image processing, implemented on a standard industrial programmable logic controller, it is possible to stabilize the upper ball with both measurement types.

Keywords: Ball on Ball, Nonlinear control, Vision based measurement, Programmable logic controller

1. Introduction

Vision based measurement is getting increasingly important in automation systems. Examples are object recognition to grab objects with a robot [1] or obstacle recognition for path planning of autonomous moving systems [2]. As the computing power of modern processors is continuously increasing, it is possible to use vision based methods for position detection.

The main idea of this work is to stabilize a ball on top of another ball by means of vision-based feedback via a programmable logic controller (PLC). Ball on ball control has been reported in literature by using two bowling balls of the same size stabilizing the upper ball [3], with position measurement done by two triangulation sensors. Another ball on ball setup has been reported [4] [5], where the lower ball is 9 times bigger than the upper ball. In this setup the position measurement is done with a 128x101 pixel CMOS sensor. The image processing to determine the upper ball position is done on a FPGA.

The contribution of this paper is the demonstration of feasibility of performing control and image processing for a ball on ball setup on a standard industrial PLC. Due to the implementation of direct access to the camera in the used PLC system, the image processing can be done entirely on the PLC.

In Sec. 2 the modeling of the mechanical and the electrical system is done. The controllers to stabilize the system are designed in Sec. 3. Sec. 4 shows the experimental setup and parameters. The results are shown in Sec. 5 and are concluded in Sec. 6.

2. Modeling of the system

2.1 Mechanical system In Fig. 1 the schematic structure of the system is shown. The coordinate systems are labeled cf_i, where i denotes the number of the coordinate

a) Correspondence to: matthias.bibl@tuwien.ac.at
 * Automation and Control Institute, Vienna University of Technology, Gußhausstraße 27-29, A-1040 Vienna, Austria
 ** Beckhoff Automation GmbH
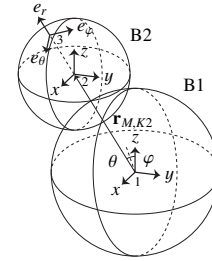   Schloss 2B/Top 3, A-2542 Kottingbrunn, Austria

Fig. 1. Schematic of the lower (B1) and the upper (B2) ball with the coordinate systems and the model variables.

system in the drawing. To derive the equations of motion the Euler-Lagrange equation is used. The dynamics of the balls are calculated in their respective body coordinate systems $cf_i, i \in [1, 2]$ and are then transformed into the same coordinate system. To describe the rotation of both balls Euler angles are used and the order of rotations is chosen to the z'xz-convention [6]. With the Euler angles of the i-th ball $(\alpha_i, \beta_i, \gamma_i)$ the full rotation matrix can be found as

$$\mathbf{R}_{z'xz} = \mathbf{R}_{z'}(\alpha_i) \cdot \mathbf{R}_x(\beta_i) \cdot \mathbf{R}_z(\gamma_i) =$$

$$\begin{pmatrix} c_{\alpha,i}c_{\gamma,i} - s_{\alpha,i}c_{\beta,i}s_{\gamma,i} & s_{\alpha,i}c_{\gamma,i} + c_{\alpha,i}c_{\beta,i}s_{\gamma,i} & s_{\beta,i}s_{\gamma,i} \\ -c_{\alpha,i}s_{\gamma,i} - s_{\alpha,i}c_{\beta,i}c_{\gamma,i} & -s_{\alpha,i}s_{\gamma,i} + c_{\alpha,i}c_{\beta,i}c_{\gamma,i} & s_{\beta,i}c_{\gamma,i} \\ s_{\alpha,i}s_{\beta,i} & -c_{\alpha,i}s_{\beta,i} & c_{\beta,i} \end{pmatrix} \quad (1)$$

with the cosine $c_{x,i}$ and the sine $s_{x,i}$ of the angle x_i.

The kinetic energy of both balls, which is needed for the Euler-Lagrange equation, can be found by the skew-symmetric matrix $\mathbf{S}$ [7] and is given by

$$\mathbf{S} = \dot{\mathbf{R}}\mathbf{R}^T = \begin{pmatrix} 0 & -\omega_z & \omega_y \\ \omega_z & 0 & -\omega_x \\ -\omega_y & \omega_x & 0 \end{pmatrix}. \quad (2)$$

So the angular velocities can be determined to

$$\omega_x = \sin(\alpha)\sin(\beta)\dot{\gamma} + \cos(\alpha)\dot{\beta} \quad (3a)$$

$$\omega_y = -\cos(\alpha)\sin(\beta)\dot{\gamma} + \sin(\alpha)\dot{\beta} \quad (3b)$$

$$\omega_z = \dot{\alpha} + \cos(\beta)\dot{\gamma}. \quad (3c)$$

By using a transformation to the coordinate system cf_3 the coordinate systems can be brought to the same coordinate system. When assuming that each of the two balls is axially symmetric the moment of inertia for each ball is given by

$$I_i = \frac{2}{5}m_i r_i^2, \tag{4}$$

where m_i denotes the mass of the ball and r_i the radius of the ball. The potential and kinetic energy of the balls can be found, where the potential energy of the lower ball is zero because it can only make rotational but no translational movements.

Two boundary conditions for the system can be determined. The first one is that the upper ball is always on top of the lower ball, so the distance between the centers of the two balls is always the sum of the radii of the two balls. So the first condition is

$$|\mathbf{r}_{M,K2}| = \sqrt{x^2 + y^2 + z^2} = \sqrt{(r_1 + r_2)^2} = R. \tag{5}$$

The second boundary condition is, that assuming there is no slip between the balls, the rolling condition

$$\mathbf{r}_2 \times \omega_2 + \mathbf{v} = \mathbf{r}_1 \times \omega_1 \tag{6}$$

with the vector of the angular velocities ω_i of the balls and the translational velocity $\mathbf{v}$ of the upper ball, has to be fulfilled.

The generalized coordinates are chosen to be

$$\mathbf{q} = \begin{bmatrix} \alpha_1 & \beta_1 & \gamma_1 & \varphi & \theta & \alpha_2 & \beta_2 & \gamma_2 \end{bmatrix}^T, \tag{7}$$

with the Euler angles α_i, β_i and γ_i of each ball, the generalized velocities are

$$\dot{\mathbf{q}} = \begin{bmatrix} \omega_{1,\varphi} & \omega_{1,\theta} & \omega_{1,r} & \omega_\varphi & \omega_\theta & \omega_{2,\varphi} & \omega_{2,\theta} & \omega_{2,r} \end{bmatrix}^T, \tag{8}$$

and the generalized forces are

$$\tau = \begin{bmatrix} M_1 & M_2 & 0 & 0 & 0 & 0 & 0 & 0 \end{bmatrix}^T. \tag{9}$$

By using the Euler-Lagrange equation

$$\frac{d}{dt}\left(\frac{dL}{d\dot{q}_j}\right) - \frac{dL}{dq_j} = \tau \tag{10}$$

with the Lagrangian

$$L = T_{K1} + T_{K2} - V_{K1} - V_{K2}, \tag{11}$$

where T denotes the kinetic energy of the balls and V the potential energy and by using the Euler-Lagrange equation of the first kind the term

$$\mathbf{A}(\mathbf{q})\lambda = \sum_i \frac{\partial f_i}{\partial \dot{q}_j}\lambda_i \,, i \in k \tag{12}$$

can be found and added to Eq. 10 to consider the k boundary conditions of Eqs. (5) and (6). The resulting system can be written as

$$\dot{\mathbf{x}} = \begin{pmatrix} \frac{\lambda_2 r_1}{I_1} \\ \frac{-\lambda_1 r_1}{I_1} \\ 0 \\ \omega_\varphi \\ \omega_\theta \\ \frac{2m_2\omega_\varphi\omega_\theta(r_1+r_2)\sin(\theta)+m_2 g\sin(\varphi)-\lambda_2}{(r_1+r_2)\cos(\theta)m_2} \\ \frac{m_2(-\omega_\varphi^2(r_1+r_2)\cos(\theta)+g\cos(\varphi))\sin(\theta)+\lambda_1}{(r_1+r_2)m_2} \\ \frac{\lambda_2 r_2}{I_2} \\ -\frac{\lambda_1 r_2}{I_2} \\ 0 \end{pmatrix} + \begin{pmatrix} \frac{1}{I_1} \\ 0 \\ 0 \\ 0 \\ 0 \\ 0 \\ 0 \\ 0 \\ 0 \\ 0 \end{pmatrix} M_1 + \begin{pmatrix} 0 \\ \frac{1}{I_1} \\ 0 \\ 0 \\ 0 \\ 0 \\ 0 \\ 0 \\ 0 \\ 0 \end{pmatrix} M_2 \tag{13}$$

with the boundary conditions

$$0 = r_1\omega_{1,\theta} - (r_1 + r_2)\omega_\theta + r_2\omega_{2,\theta} \tag{14a}$$

$$0 = -r_1\omega_{1,\varphi} + \cos(\theta)(r_1 + r_2)\omega_\varphi - r_2\omega_{2,\varphi} \tag{14b}$$

and the state vector

$$\mathbf{x} = \begin{bmatrix} \omega_{1,\varphi} & \omega_{1,\theta} & \omega_{1,r} & \varphi & \theta & \omega_\varphi & \omega_\theta & \omega_{2,\varphi} & \omega_{2,\theta} & \omega_{2,r} \end{bmatrix}^T. \tag{15}$$

As the angular velocities $\omega_{2,\varphi}$ and $\omega_{2,\theta}$ can not be measured and are not needed for the control task their dynamic equations are solved for the lagrange multipliers. By differentiating with respect to time the terms can be substituted in Eq. (13) and the final form can be found. Because of the fairly large result the final result is not shown.

2.2 Electrical System The lower ball is driven by three permanent magnet synchronous motors (PSM). The model of the PSM is [8]

$$\dot{\mathbf{x}} = \begin{pmatrix} \frac{1}{l_s}(-i_{sd}r_s + \omega_m l_s i_{sq}) \\ \frac{1}{l_s}(-i_{sq}r_s - \omega_m(l_s i_{sd} + \Psi_M)) \\ \frac{1}{\tau_m}(i_{sq}\Psi_M + \tau_L) \end{pmatrix} + \begin{pmatrix} \frac{1}{l_s} \\ \frac{1}{l_s} \\ 0 \end{pmatrix} \begin{bmatrix} u_{sd} \\ u_{sq} \\ 0 \end{bmatrix} \tag{16a}$$

$$y = i_{sq}\Psi_M, \tag{16b}$$

where l_s denotes the stator inductance, r_s is the stator resistance Ψ_M is the interlinking magnetic flux and τ_L is the load moment. The state vector $\mathbf{x} = \begin{bmatrix} i_{sd} & i_{sq} & \omega_m \end{bmatrix}$ denotes the stator current i in d and q direction and the rotational speed ω_m. The input of the system is the stator voltage u in d and q direction and the output is the mechanical torque $y = \tau_M$.

It can be assumed that the mechanical system is much slower than the electrical electrical system. When using the singular perturbation method [9] by choosing the disturbance parameter $\epsilon = l_s = 0$ the model for the PSM can be reduced to the algebraic equations

$$i_{sd} = \frac{u_{sd}}{r_s}, \tag{17}$$

$$i_{sq} = \frac{u_{sq} - \Psi_M\omega_m}{r_s} \quad \text{and} \tag{18}$$

$$\tau_m = \frac{\Psi_M u_{sq} - \Psi_M^2\omega_m}{r_s}. \tag{19}$$

When adding the time constant of the rotor inertia as a second disturbance parameter Eq. (19) can be reduced to

$$\tau_m = -\tau_L. \tag{20}$$

This means that the electric subsystem is a through connection because it is much faster than the mechanical one.

2.3 Input Transformation In Eq. (13) the system inputs are the torques M_1 and M_2. In this publication the angular velocities of the lower ball are controlled and not the torques, such that an input transformation has to be found. By solving the system model of Sec. 2.1 for the torques M_1 and M_2 and substituting the remaining equations the new system with the inputs $\omega_{1,\varphi}$ and $\omega_{1,\theta}$ is found. Since the two states $\omega_{1,r}$ and $\omega_{2,r}$ do not influence any other states and can not be actuated or measured they are neglected. When all higher terms of ω_φ and ω_θ are neglected the system can be reduced

to

$$\mathbf{f}(\mathbf{x}, \mathbf{u}) = \begin{pmatrix} \omega_\varphi + \frac{I_2 r_1}{(r_1+r_2)(m_2 r_2^2+I_2)\cos(\theta)}\omega_{1,\varphi} \\ \omega_\theta + \frac{I_2 r_1}{(r_1+r_2)(m_2 r_2^2+I_2)}\omega_{1,\theta} \\ \frac{gm_2 r_2^2 \sin(\varphi)}{(r_1+r_2)(m_2 r_2^2+I_2)\cos(\theta)} \\ \frac{g\cos(\theta)m_2 r_2^2 \sin(\theta)}{(m_2 r_2^2+I_2)(r_1+r_2)} \end{pmatrix}. \tag{21}$$

Assuming that the angles φ and θ are small, the simplification $\cos(\theta) \approx 0$ can be used and the system

$$\mathbf{f}(\mathbf{x}, u) = \underbrace{\begin{pmatrix} \omega_\varphi \\ \frac{gm_2 r_2^2 \sin(\varphi)}{(r_1+r_2)(m_2 r_2^2+I_2)} \end{pmatrix}}_{\mathbf{f}(\mathbf{x})} + \underbrace{\begin{pmatrix} \frac{I_2 r_1}{(r_1+r_2)(m_2 r_2^2+I_2)} \\ 0 \end{pmatrix}}_{\mathbf{g}(\mathbf{x})} u, \tag{22}$$

with the reduced state vector $\mathbf{x} = \begin{bmatrix} \varphi & \omega_\varphi \end{bmatrix}^T$ can be found. This system is valid for the φ and the θ angle. So the system splits into two indentical decoupled systems around the upper rest position.

2.4 Linearisation For a first analysis the system of Eq. (21) is linearized around the upper rest position where $\varphi = \theta = 0$ and $\dot{\mathbf{x}}_{u=0} = \mathbf{0}$. The system can be determined as

$$\mathbf{A} = \begin{pmatrix} 0 & 0 & 1 & 0 \\ 0 & 0 & 0 & 1 \\ a_1 & 0 & 0 & 0 \\ 0 & a_1 & 0 & 0 \end{pmatrix}, \text{ with} \tag{23a}$$

$$a_1 = \frac{gm_2 r_2^2}{(r_1+r_2)(m_2 r_2^2+I_2)} \tag{23b}$$

and the input matrix

$$\mathbf{B} = \begin{pmatrix} b_1 & 0 \\ 0 & b_1 \\ 0 & 0 \\ 0 & 0 \end{pmatrix}, \text{ with} \tag{24a}$$

$$b_1 = \frac{I_2 r_1}{(m_2 r_2^2+I_2)(r_1+r_2)}. \tag{24b}$$

It can easily be seen that also the linearized system splits into two identical systems of the form

$$\dot{\mathbf{x}} = \begin{pmatrix} 0 & 1 \\ a_1 & 0 \end{pmatrix}\mathbf{x} + \begin{pmatrix} b_1 \\ 0 \end{pmatrix}u \tag{25a}$$

$$y = \underbrace{\begin{pmatrix} 1 & 0 \end{pmatrix}}_{\mathbf{C}}\mathbf{x} + \underbrace{\mathbf{0}}_{\mathbf{D}}u. \tag{25b}$$

with the state vectors $\mathbf{x}_1 = \begin{bmatrix} \varphi & \omega_\varphi \end{bmatrix}^T$ and $\mathbf{x}_2 = \begin{bmatrix} \theta & \omega_\theta \end{bmatrix}^T$. The resulting system is much easier to analyse. It can be shown that each subsystem has a pole in the left half-plane and one in the right half-plane. A pole zero map of the linearized system is shown in Fig. 2. The observability matrix $\mathscr{O}(\mathbf{A}, \mathbf{C}) = \begin{bmatrix} \mathbf{C} & \mathbf{CA} \end{bmatrix}^T$ has full rank $n = 2$, even if the angular velocity $\omega_{1,\varphi}$ can not be measured, therefore the system is fully observable. Also the controllability matrix $\mathscr{R}(\mathbf{A}, \mathbf{B}) = \begin{bmatrix} \mathbf{B} & \mathbf{AB} \end{bmatrix}$ has full rank and therefore the system is fully controllable. Due to the decoupling of the two axes a controller can be designed for one axis and then also be used for the second axis.
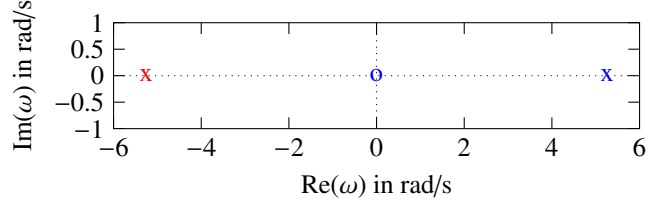

Fig. 2. Pole zero map of the linearized system of Eq. (25). Due to the pole in the right half plane the system is unstable.
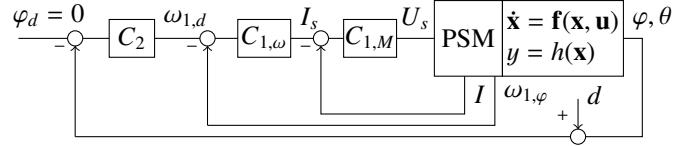

Fig. 3. Used control structure to stabilize the system. The two inner loops control the PSM current and angular velocity, the outer loop controls the angle of the upper ball.

3. Control Design

Based on the derived mathematical model a controller is designed to stabilize the upper ball in the upper rest position. In Table 1 the used parameters for the system are given. The

Table 1. Model parameters used for the simulation.

Parameter	Value
r_1	150 mm
r_2	100 mm
m_1	5 kg
m_2	3 kg
M_{max}	5 Nm

control layout can be seen in Fig. 3, where φ_d denotes the desired angle of the upper ball, $\omega_{1,d}$ is the desired velocity of the upper ball, I_s is the current, and U_s the voltage of the PSM.

3.1 Linear Controller Design Using the parameters of Table 1 the system dynamics of Eq. (25) leads to

$$\dot{\mathbf{x}}_1 = \begin{pmatrix} 0 & 1 \\ 28.03 & 0 \end{pmatrix}\mathbf{x}_1 + \begin{pmatrix} 0.1714 \\ 0 \end{pmatrix}u \tag{26a}$$

$$\mathbf{y}_1 = \begin{pmatrix} 1 & 0 \end{pmatrix}\mathbf{x}_1. \tag{26b}$$

This system is used for the linear control design.

Because of the integrating behavior of the system a PD controller in generalized system coordinates of the form

$$\tau = \mathbf{K_p}(\mathbf{q}_d - \mathbf{q}) - \mathbf{K_d}\dot{\mathbf{q}} + \mathbf{g}(\mathbf{q}), \tag{27}$$

with $\mathbf{K_p}$ beeing the proportional gain matrix, $\mathbf{K_D}$ the differential gain matrix, $\mathbf{g}(\mathbf{q})$ the compensation term for potential forces, and the desired coordinates $\mathbf{q}_d$, is sufficient to stabilize the unstable upper rest position. To design the PD control the tuning rule presented in [10] is used. By choosing a crossover frequency of $\omega_C = 35\,\mathrm{s}^{-1}$ and empirical optimization of the gain $K_d = 11$, the system can be stabilized. The response of
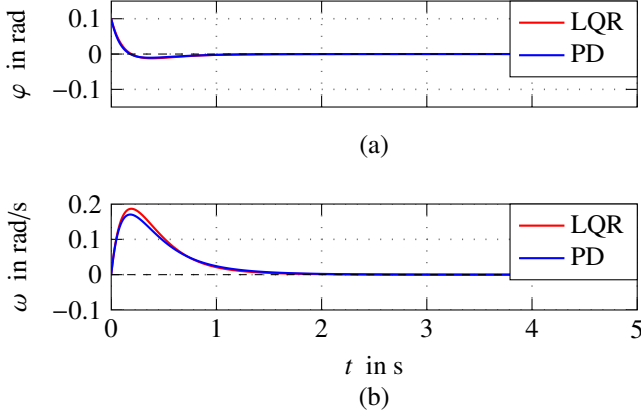
Fig. 4. Angle φ of the upper ball over time for a initial deflection of $\varphi_0 = 0.1$ rad (a) and the corresponding angular velocity $\omega_{1,\varphi}$ (b).

the system is shown in Fig. 4 (blue) for a initial deflection of 0.1 rad.

A second method to stabilize the upper rest position is the linear quadratic regulator (LQR) [11]

$$u_k = -\mathbf{K}\mathbf{x}_k. \tag{28}$$

The LQR is designed directly for the time discrete system and therefore a sampling time has to be chosen, such that the sampling frequency is 5 to 25 times higher than the system bandwidth [11][12]. This leads to a sampling time between 86 ms and 17 ms. As the PLC can easily achieve a sampling time of 10 ms for the implementation, a sampling time of 10 ms is chosen. The discretised system is given by

$$\mathbf{x}_{1,k+1} = \underbrace{\begin{pmatrix} 1.001 & 0 \\ 0.2804 & 1.001 \end{pmatrix}}_{\mathbf{\Phi}} \mathbf{x}_{1,k} + \underbrace{\begin{pmatrix} 0.001715 \\ 0.0002405 \end{pmatrix}}_{\mathbf{\Gamma}} u_k \tag{29a}$$

$$\mathbf{y}_{1,k} = \underbrace{\begin{pmatrix} 1 & 0 \end{pmatrix}}_{\mathbf{C}} \mathbf{x}_{1,k}. \tag{29b}$$

By using the cost function

$$J = \sum_{k=0}^{N-1} (\mathbf{x}_k^T \mathbf{Q} \mathbf{x}_k + \mathbf{u}_k^T \mathbf{R} \mathbf{u}_k + 2\mathbf{x}_k^T \mathbf{N} \mathbf{u}_k) + \mathbf{x}_N^T \mathbf{S} \mathbf{x}_N \tag{30}$$

with the weighting matrices $\mathbf{Q}, \mathbf{R}, \mathbf{N}$ and $\mathbf{S}$ with respect to $\mathbf{u}_{N-1}$ and the weighting matrices

$$\mathbf{Q} = \begin{pmatrix} 7000 & 0 \\ 0 & 1 \end{pmatrix}, R = 10 \text{ and } \mathbf{N} = \mathbf{0} \tag{31}$$

the feedback gain vector

$$\mathbf{k} = \begin{pmatrix} 65.0452 & 11.3482 \end{pmatrix} \tag{32}$$

can be found. This feedback vector is similar to the previously designed PD controller [10]. In Fig. 4 the response of the system to an initial deflection of 0.1 rad (red) is shown.

3.2 Nonlinear Controller Design A third control strategy is to design a nonlinear controller for the system of Eq. (22). As discussed earlier the coupling between the orthogonal axes is weak and therefore the system can be seen

as two orthogonal ball on wheel systems. It can be shown that a ball on wheel system with the torque as input is flat [13]. A system that can be linearized by feedback must have the form [9]

$$\dot{\mathbf{x}} = \mathbf{A}\mathbf{x} + \mathbf{B}\gamma(\mathbf{x})(u - \alpha(\mathbf{x})) \tag{33}$$

which is the case for Eq. (22). To verify that a flat output exists the matrix

$$\mathbf{G} = \begin{bmatrix} \mathbf{g} & \mathbf{L_f g(x)} \end{bmatrix} = \begin{pmatrix} \frac{I_2 r_1}{(r_1+r_2)(m_2 r_2^2 + I_2)} & 0 \\ 0 & -\frac{g m_2 r_2^2 I_2 r_1 \cos(\varphi)}{(r_1+r_2)^2 (m_2 r_2^2 + I_2)^2} \end{pmatrix} \tag{34}$$

with $\mathbf{f}$ and $\mathbf{g}$ from Eq. (22) must have full rank. As this is true it remains to show that the distribution $D = \text{span}\{\mathbf{g}\}$ is involute in an area around $\bar{\mathbf{x}}$. Because D has full rank the distribution is a basis of the complete $\mathbb{R}$, and therefore the Lie-brackets of every combination $\mathbf{f_i(x)}, \mathbf{f_j(x)} \in D$ of vector fields has to fulfill $[\mathbf{f_i(x)}, \mathbf{f_j(x)}] \in D$. Therefore it is shown that the system must have an output with relative order $r = n$. A possible flat output is simply found by

$$y = h(\mathbf{x}) = \omega_\varphi. \tag{35}$$

By differentiating the output it can be shown that $\dot{y}$ is independent of the input $\omega_{1,\varphi}$, but $\ddot{y}$ is function of $\omega_{1,\varphi}$. Because the input occurs at the second derivative the relative order r is 2, which is also the number of system states, such that the output is flat. This means a feedback law according to the form of [9]

$$u = \frac{1}{\mathbf{L_g} h(x)}(-\mathbf{L_f} h(x) + v) \tag{36}$$

can be derived. To set a desired characteristic polynomial of the linearized system the new input v is chosen to be

$$v = -\sum_{j=1}^{n} a_{j-1} \mathbf{L_f}^{j-1} h(\mathbf{x}). \tag{37}$$

This results in a denominator of the form $s^r + a_{r-1} s^{r-1} + ... a_0$ and the complete feedback law is given by

$$u = \frac{1}{\mathbf{L_g L_f} h(\mathbf{x})}(-\mathbf{L_f}^2 h(\mathbf{x}) + v) = \tag{38}$$

$$-\frac{7}{2} \frac{(r_1 + r_2)[m_2 g \cos(\varphi) r_2^2 \omega_\varphi + a_1 m_2 g \sin(\varphi) r_2^2 +}{m_2 g r_2^2 r_1 \cos(\varphi)}$$

$$\frac{(r_1 + r_2)(m_2 r_2^2 + I_2)(a_0 \omega_\varphi - v)]}{},$$

with the coefficients a_j of the desired characteristic polynomial. The coefficients are chosen to (12, 36) and the resulting poles of the transfer function are $(-6, -6)$, because these parameters yield good results in the simulation. The system response for a initial deflection of 0.1 rad can be seen in Fig. 5 (red) in comparison to the LQR controller (dashed blue).

The three designed controllers are designed for the simplified system models. To quantify the error by these simplifications the simulations are done for the reduced and the full nonlinear model. It turns out that the behavior for the angle is nearly identical and for the angular velocities a small
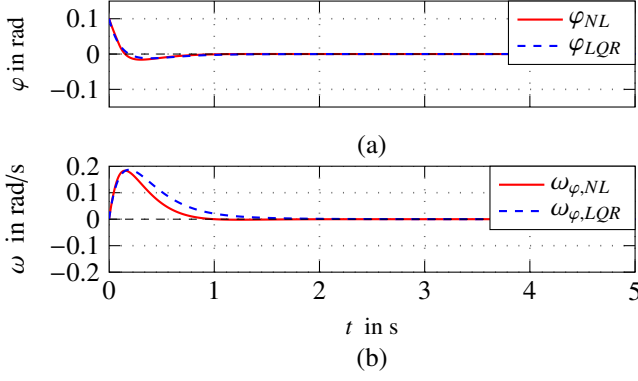
Fig. 5. Angle φ of the upper ball over time for a initial deflection of $\varphi_0 = 0.1$ rad (a) and the corresponding angular velocity $\omega_{1,\varphi}$ (b).
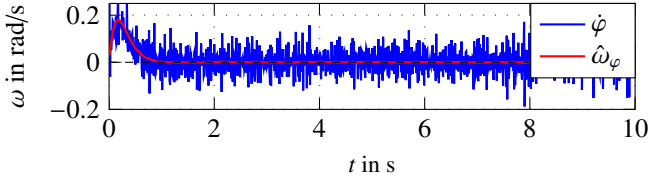

Fig. 6. The derivative of the angle φ compared to the estimated state $\hat{\omega}_\varphi$.

Table 2. Parameters of the lower and the upper ball.

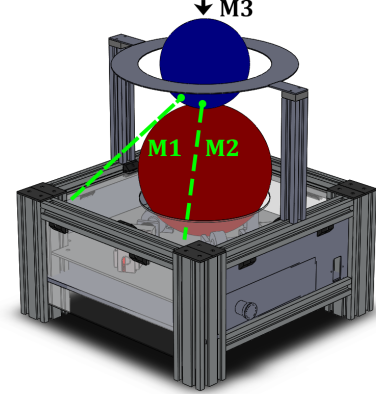| Parameter	Value
m_1	1.40 kg
m_2	3.56 kg
r_1	151 mm
r_2	101 mm

Fig. 7. Sketch of the experimental setup. The dashed green lines indicate the laser beam of the triangulation sensors and the black arrow indicates the camera view.

deviation at the peak velocity can be seen (data not shown). Therefore it is concluded that the controllers designed for the reduced system also work for the full nonlinear system.

3.3 State Observer It was assumed that all system states can be measured. This is true for the angles φ and θ but not for the angular velocities ω_φ and ω_θ. To determine the velocities the angles can be differentiated with respect to time. This method is known to amplify measurement noise and may not provide good results. A different method is to use a state observer in form of a Kalman filter [14]. For the linear Kalman filter the matrices $\mathbf{Q}$, $\mathbf{R}$ and $\mathbf{N}$ need to be chosen, as well as the initial state of $\hat{\mathbf{x}}_0$. The filter is designed for the time-discrete system from Eq. (29). Furthermore the system is extended by the disturbance $\mathbf{w}_k$ and the sensor noise $\mathbf{v}_k$, and the matrices $\mathbf{G}$ and $\mathbf{H}$ are chosen to

$$\mathbf{G} = \begin{pmatrix} 0.25 \\ 1 \end{pmatrix} \text{ and } H = 0 \qquad (39)$$

so the disturbance mainly influences the not measured state ω_φ. The disturbance $\mathbf{w}_k$ and the sensor noise $\mathbf{v}_k$ are assumed as one dimensional properties and their covariance matrices $\mathbf{Q}$ and $\mathbf{R}$ are therefore scalars. They are tuned empirically to

$$Q = 500000 \text{ and } R = 7. \qquad (40)$$

This leads to the estimation matrix

$$L = \begin{pmatrix} 0.5249 \\ 2.2480 \end{pmatrix}. \qquad (41)$$

With these settings the Kalman filter achieves a good estimation of the state vector, even if the measurement noise is large, which can be seen in Fig. 6.

4. Experimental Setup

After modeling the system and designing the controllers a experimental setup is built. The parameters of the setup are shown in Table 2. A CAD sketch of the final setup can be seen in Fig. 7. The setup is driven by three Beckhoff PSM servo Motors AM8121 with a max. torque of 0.5 Nm. To increase the torque a Beckhoff AG2250 gearbox with a gear ratio of 1:3 is used. The gearbox is via a flexible jaw coupling connected with an omniwheel to drive the lower ball. A Beckhoff EL7211-9014 inverter is used to control the current and the angular velocity of each motor. TwinCAT from Beckhoff is used as the PLC software and the used industrial PC is a Beckhoff CX2030. The controllers are implemented in Matlab Simulink and then exported as a C++ object. These objects can be directly imported and used in TwinCAT.

4.1 Triangulation Measurement (M1 & M2) To determine the position of the upper ball two triangulation sensors IL 300 from Keyence are used. The two triangulation sensors measure the distance to the upper ball from which the the angle φ and θ can be calculated. In principle the task of calculating the two angles can be reduced to the task of finding the intersection of three spheres and is known as trilateration [15].

4.2 Camera Based Measurement (M3) To detect the upper ball position also an industrial gigabit ethernet camera Manta G046C is used. It is mounted above the upper ball, so that the full ball and its movement can be observed. The camera is connected to the PLC and the images are directly transferred. Beckhoff TwinCAT vision module is used to calculate the position and the angles of the upper ball. As the lower ball is white and the upper ball red, it is the most intuitive approach to use just the red color channel of the RGB image to detect the center of mass of the ball and calculate the angles. This method is quite robust against wrong color pixels as they don't really influence the center of mass due to averaging. When the illumination is changed due to different light conditions also the thresholds for the red detec-
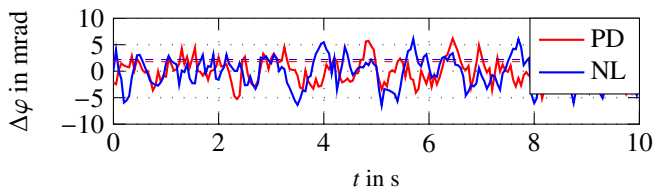
Fig. 8. Residual control error of the PD control (1.80 mrad RMS) and the nonlinear control (2.20 mrad RMS). RMS values are drawn dashed.
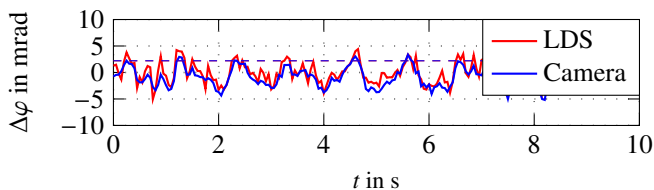

Fig. 9. Residual control error of the laser distance sensors (2.20 mrad RMS) and the camera (2.21 mrad RMS) using nonlinear control. RMS values are drawn dashed.

tion have to change multiple times a day. This leads to a weak contour detection and therefore to an unreliable measurement. The calculation duration for the selected image size of 580x580 pixel is about $650\,\mu s$.

To get a more reliable measurement the RGB image is transformed to the Hue Saturation Value (HSV) color space with the brightness as parameter [16]. The transformation of the image to the HSV space has a duration of about 2 ms. To decrease this time not the full image ins transformed, instead two stripes around the rest position in orthogonal directions are taken from the image and transformed. After the transformation the color detection and the mass center detection are done in the HSV color space. The whole optimized procedure takes about $800\,\mu s$.

5. Results

In Fig. 8 the residual error of the stabilized system can be seen. The system can be stabilized with the PD and the nonlinear controller with a sample time of 10 ms. It can be seen, that the RMS error of both control methods is nearly the same. To evaluate the performance of the vision feedback the stabilization of the upper ball is done with the nonlinear controller and the camera measurement. The result can be seen in Fig. 9. The nonlinear controller with camera feedback (blue) shows the same performance for a sampling time of 10 ms as the nonlinear controller with the laser distance sensors (LDS). The total sampling time of the camera position measurement is approx. 9.5 ms while the LDS needs approx. 3 ms which can clearly be seen in Fig. 9.

To show the disturbance rejection a pneumatic actuator is mounted on the system to get a reproducible disturbance for the upper ball position. The angular disturbance is about 13.8 mrad at 3.6 s. The reaction of the system on a disturbance can be seen in Fig. 10. The RMS values of the controller with the LDS measurement and the vision measurement are nearly equal and with both measurement methods the NL controller is able to keep the upper ball on top of the lower ball.
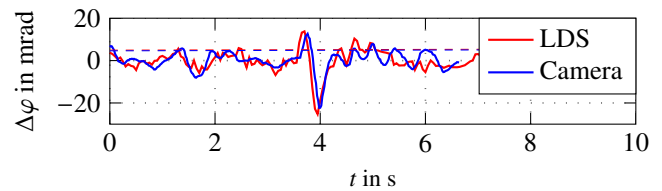

Fig. 10. Disturbance reaction by a pneumatic actuator at 3.6 s of the NL control using LDS (4.91 mrad RMS) and camera position measurement (4.61 mrad RMS). RMS values are drawn dashed.

6. Conclusion

In this work a ball on ball setup is modeled, and linear and nonlinear controllers are designed and implemented. The measurement of the upper ball position is done with LDS and camera based. A state observer is introduced to determine the angular velocities of the upper ball. The experiments on the built setup show that it is possible to stabilize the ball on ball system with both feedback systems with a similar performance, and also a good disturbance rejection can be achieved. The complete control task and the image processing being performed on a PLC has been successfully demonstrated.

Acknowledgment

References

(1) A. J. Koivo and N. Houshangi, "Real-time vision feedback for servoing robotic manipulator with self-tuning controller," *IEEE Transactions on Systems, Man, and Cybernetics*, vol. 21, no. 1, pp. 134–142, 1991.

(2) M. Bertozzi and A. Broggi, "Gold: A parallel real-time stereo vision system for generic obstacle and lane detection," *IEEE Transactions on Image Processing*, vol. 7, no. 1, pp. 62–81, 1998.

(3) R. Gahleitner, "Ball on ball: Modeling and control of a novel experiment set-up," *IFAC-PapersOnLine*, vol. 48, pp. 796–801, 2015.

(4) Shih-Yuan Liu, Yusie Rizal, and Ming-Tzu Ho, "Stabilization of a ball and sphere system using feedback linearization and sliding mode control," in *8th Asian Control Conference*, 2011.

(5) Ming-Tzu Ho, Yusie Rizal, and Wen-Shen Cheng, "Stabilization of a vision-based ball-on-sphere system," in *IEEE International Conference on Control Applications*, 2013.

(6) H. Goldstein, J. C. P. Poole, and S. J. L. Safko, *Klassische Mechanik*. Wiley-VCH, 2012.

(7) B. Siciliano, L. Sciavicco, L. Villani, and G. Oriolo, *Robotics - Modeling, Planning and Control*. Springer Verlag, 2009.

(8) R. Fischer, *Elektrische Maschinen*. Hanser Fachbuchverlag, 2003.

(9) H. K. Khalil, *Nonlinear Systems (3rd edition)*. Pearson, 2001.

(10) R. Munnig Schmidt, G. Schitter, and J. van Eijk, *High Performance Mechatronics*. Delft University Press, 2011.

(11) G. F. Franklin, J. D. Powell, and M. L. Workman, *Digital Control of Dynamic Systems*. Addison Wesley Longman, 1998.

(12) I. D. Landau and G. Zito, *Digital Control Systems*. Springer Verlag, 2005.

(13) S. Fuchshumer, K. Schlacher, G. Grabmair, and K. Straka, "Flachheits-basierte Folgeregelung des Labormodells Ball on the Wheel," *e&i*, no. 9, pp. 301–306, 2004.

(14) R. E. Kalman, "A new approach to linear filtering and prediction problems," *Transaction of the ASME, Journal of Basic Engineering*, pp. 35–45, 1960.

(15) F. Thomas and L. Ros, "Revisiting trilateration for robot localization," *IEEE Transactions on Robotics*, vol. 21, no. 1, pp. 93–101, 2005.

(16) A. R. Smith, "Color gamut transform pairs," *ACM SIGGRAPH Computer Graphics*, vol. 12, no. 3, pp. 12–19, 1978.